Chinese Chemical Letters 33 (2022) 3231–3235

Contents lists available at ScienceDirect

Chinese Chemical Letters

journal homepage: www.elsevier.com/locate/cclet

Waste-yeast biomass as nitrogen/phosphorus sources and carbon template: Environment-friendly synthesis of N,P-Mo_2C nanoparticles on porous carbon matrix for efficient hydrogen evolution

Jiayuan Yu[a,b], Wanqiang Yu[a], Bin Chang[a], Xiao Li[a,*], Jin Jia[a,*], Dufu Wang[b], Zhinian Xu[b], Xiaoli Zhang[c], Hong Liu[a,d], Weijia Zhou[a,*]

[a] *Collaborative Innovation Center of Technology and Equipment for Biological Diagnosis and Therapy in Universities of Shandong, Institute for Advanced Interdisciplinary Research (iAIR), University of Jinan, Ji'nan 250022, China*
[b] *Shandong Best Environmental Technology Co., Ltd., Ji'nan 250101, China*
[c] *School of Materials Science and Engineering, Zhengzhou University, Zhengzhou 450001, China*
[d] *State Key Laboratory of Crystal Materials, Shandong University, Ji'nan 250100, China*

ARTICLE INFO

Article history:
Received 30 July 2021
Revised 23 August 2021
Accepted 17 October 2021
Available online 24 October 2021

Keywords:
Hydrogen evolution reaction
Molybdenum carbide
Non-metal doping
Resource utilization
Solid waste management

ABSTRACT

Tailor-made advanced electrocatalysts with high active and stable for hydrogen evolution reaction (HER) play a key role in the development of hydrogen economy. Herein, a N,P-co-doped molybdenum carbide confined in porous carbon matrix (N,P-Mo_2C/NPC) with a hierarchical structure is prepared by a resources recovery process. The N,P-Mo_2C/NPC compound exhibits outstanding HER activity with a low overpotential of 84 mV to achieve 10 mA/cm^2, and excellent stability in alkaline media. The electrochemical measurements confirm that the enhanced HER activity of N,P-Mo_2C/NPC is ascribe to the synergy of N,P-codoped and porous carbon matrix. Density functional theory calculations further reveal that the electron density of active sites on Mo_2C can be regulated by the N/P doping, leading to optimal H adsorption strength. In this work, the proof-of-concept resource utilization, a microorganism derived molybdenum carbide electrocatalyst for HER is fabricated, which may inaugurate a new way for designing electrocatalysts by the utilization of solid waste.

In order to solve the problems caused by overusing of high-pollution fossil energy, sustainable and environmentally friendly energies have caused widely concern from all over the world [1]. Due to its wide source, high energy density and nonpollution, hydrogen (H_2) is considered as the most prospective substitute to fossil energy [2,3]. Electrocatalytic water splitting powered by renewable energy is an efficient and sustainable approach for H_2 production [4–8]. In order to promote the industrialization of electrolytic water, it is urgent to prepare efficient electrocatalysts with low overpotential and excellent long-term stability [9,10]. At present, the most advanced HER electrocatalysts are platinum-group materials (PGMs) [11–15]. However, the high cost and low reserve of PGMs limit its large-scale utilization. Therefore, it is significant to explore earth-abundant, inexpensive, and high-efficient HER electrocatalyst [16–25].

Recently, numerous noble-free electrocatalysts have been developed as probable alternatives of Pt-based materials for HER. Particularly, transition metal-based compounds have attracted much attention due to their excellent HER performance [26–29]. Among them, molybdenum carbide (Mo_2C), with similar d-band electronic structure to Pt, is consider one of the most promising nonprecious HER electrocatalyst [26,27]. Nevertheless, the HER performance of Mo_2C is still unsatisfactory. Many researchers reported that introducing conductive support and low-electronegativity nonmetallic elements (*e.g.*, N and P) doping was an effective means to promote the HER performance of Mo_2C. For example, Wang *et al.* reported that the ultrafine Mo_2C nanoparticles composited with carbon electrocatalyst possessed the onset potential of −6 mV and Tafel slope of 41 mV/dec [28]. Hu and Dai *et al.* found that N,P-doped Mo_2C owned excellent HER performance, and the enhanced performance was derived from the synergistic coupling effect of N,P-codoped [29]. Despite these developments, the large-scale application of Mo_2C was still limited by its complex preparation process and high cost. Hence, it is of great interest in developing and exploring more efficient and economic preparation method.

* Corresponding authors.
E-mail addresses: ifc_lix@ujn.edu.cn (X. Li), ifc_jiaj@ujn.edu.cn (J. Jia), ifc_zhouwj@ujn.edu.cn (W. Zhou).

https://doi.org/10.1016/j.cclet.2021.10.046
1001-8417/

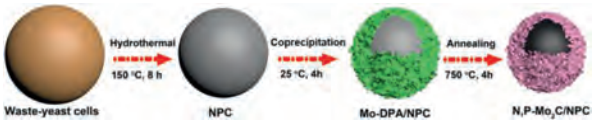

Scheme 1. Schematic diagram illustrating the upcycling waste-yeast cells to valuable N,P-Mo_2C/NPC electrocatalyst.

Microorganisms (such as bacteria, fungi and viruses) have attracted great attention in many fields owing to their accessibility, sustainability, and versatility [30]. In practice, the cell wall, membrane, nucleus, cytoplasm, vacuole, mitochondria in microorganism are rich in C, N and P elements, which can be used as biological template to synthesize heterogeneous atoms carbon-based materials and their compounds for energy storage and conversion. For instance, Asefa *et al.* prepared yeast-derived heteroatom-doped carbon microparticles as an oxygen reduction reaction electrocatalyst with high catalytic activity [31]. More recently, our group pioneered yeast as biological N, P and C source to synthesize phosphorus-doped iron nitride nanoparticles encapsulated by nitrogen-doped carbon nanosheets (P-Fe_3N@NC NSs), which possessed excellent HER performance (the overpotential to achieve the current density of 10 mA/cm^2 (η_{10}) was 102 mV).

Herein, we described a fusion of the concepts of solid waste recycling and fabrication of nonmetal doping electrocatalyst: from waste (waste-yeast-biomass) to wealth (N,P-Mo_2C/NPC as efficient electrocatalysts for HER). As expected, the optimal N,P-Mo_2C/NPC delivered an excellent HER performance ($\eta_{10} = 84$; Tafel slope = 42 mV/dec), superior to most ever-reported noble metal-free electrocatalysts in alkaline electrolytes. DFT results further identified that N/P-codoping in Mo_2C could be optimized the Mo-H strength, and enhanced the HER performance. This strategy may provide an important way to design transition-metal carbides as efficient HER electrocatalysts.

The waste-yeast cells from wine fermentation process were an attractive bio-renewable resources, which possess high surface area and abundant non-metallic elements of C, N and P. In present work, we demonstrated an environment-friendly method that used waste-yeast biomass as C, N and P sources to synthesize N/P-Mo_2C/NPC as an effective HER electrocatalyst. As depicted in Scheme 1, the waste-yeast biomass derived N/P-codoped carbon (NPC) was firstly synthesized by a hydrothermal treatment. Then, NPC was employed as support to attachment of Mo-polydopamine (Mo-DPA) nanosheets to obtain Mo-DPA/NPC microspheres with a core-shell structure. Finally, the as-prepared Mo-DPA/NPC precursor was directly annealed at 750 °C for 4 h in Ar/H_2 gas flow to obtain well-crystalline ultrafine N,P-Mo_2C NPs anchoring in the carbon matrix (N,P-Mo_2C/NPC). During this annealing process, Mo-DPA can *in situ* produce ultrafine Mo_2C nanoparticles on carbon nanosheet. At the same time, N/P source was diffused from NPC into Mo_2C at high temperature.

The morphology of the samples was firstly measured by field-emission scanning electron microscopy (FESEM), and the typical image of fresh waste-yeast cells showed a smooth surface with a size of 2-4 μm (Fig. 1a). Energy-dispersive X-ray spectroscopy (EDS) elemental mapping revealed the uniform distribution of C, N, P and O elements in entire region of waste-yeast cells (Fig. 1b), and the according contents was 58.13 wt%, 8.35 wt%, 6.82 wt% and 26.70 wt%, respectively. Due to the smooth surface of waste-yeast cells, it was not conducive for the attachment of Mo-DPA nanosheets (Fig. S1 in Supporting information). In order to make the Mo-DPA could be successfully growth on the surface, a low temperature hydrothermal pretreatment was employed. As showed in Fig. 1c, the waste-yeast cells derived brown product was confirmed to be N/P-codoped carbon (NPC) by powder X-ray diffraction (XRD) pattern (Fig. 1h) and EDS elemental mapping (Fig. S2 in Supporting information). The obtained NPC still remained ellipse morphology but the surface become coarse, which was benefited to attach of Mo-DPA nanosheets. As shown in Figs. 1d and e, the multilevel Mo-DPA nanosheets could be perfect wrapped on the surface of NPC obtaining an core-shell structure. The XRD patterns also demonstrate the successful prepared of Mo-DPA/NPC (Fig. 1h). After annealing the Mo-DPA/NPC at 750 °C for 4 h in Ar/H_2 atmosphere, well-crystalline hierarchical N,P-Mo_2C/NPC were obtained. The corresponding XRD pattern (Fig. 1h) showed that the main characteristic peaks at 34.3°, 37.9°, 39.3°, 61.5° and 74.6° could be well indexed to the (100), (002), (101), (110) and (112) crystal facets of hexagonal β-Mo_2C (JCPDS card No. 35-0787) [27,32]. The weak peak around 25° was recognized for low crystallinity graphite carbon. Raman spectroscopy was employed to further investigate the structure of N,P-Mo_2C/NPC (Fig. S3 in Supporting information). The characteristic fingerprint bands at 334, 373, 664, 817 and 988 cm^{-1} was belonged to β-Mo_2C, [33] and the peaks at 1343 and 1603 cm^{-1} indicated the exited of defect-induced and the ordered structure of graphite carbon [34,35]. The large specific value of I_D/I_G indicated the abundant defects in graphite carbon. The FESEM images of N,P-Mo_2C/NPC (Figs. 1f and g) showed that the morphology of Mo-DPA/NPC was maintained except for a slight shrinkage, and the smooth Mo-DPA nanosheets was transformed into pore nanosheets. Fig. 1i showed the N_2 adsorption/desorption isotherms of NPC, Mo-DPA/NPC and N,P-Mo_2C/NPC, and the Brunauer–Emmett–Teller surface area was calculated to be 27.6, 35.7, 64.4 m^2/g, respectively. The pore-size distribution curve (inset in Fig. 1i) showed the existence of abundant mesopore with the diameter less than 10 nm in N,P-Mo_2C/NPC.

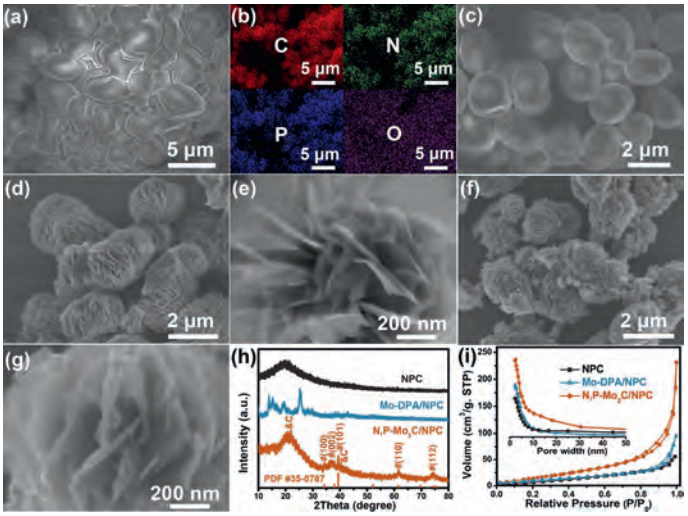

Fig. 1. FESEM and EDS elements mapping images of (a, b) pristine waste-yeast cells, (c) NPC, (d, e) Mo-DPA/NPC and (f, g) N,P-Mo2C/NPC. (h) XRD patterns and (i) Brunauer–Emmett–Teller N_2-sorptometry.

Transmission electron microscopy (TEM) was further used to acquire the fine structure of Mo-DPA/NPC and N,P-Mo_2C/NPC. The typical TEM images of Mo-DPA/NPC in Figs. 2a and b revealed that a number of Mo-DPA nanosheets (the low contrast area) were coated on the NPC core, and the thickness of the cladding layer was measured to be ~100 nm. Low crystallinity nature of Mo-DPA nanosheets were confirmed by the selected area electron diffraction (SAED) pattern (inset in Fig. 2b) and high-resolution (HR) TEM images (Fig. 2c). After calcination treatment of Mo-DPA/NPC, the TEM images in Figs. 2d-f showed that the morphology of the resultant N,P-Mo_2C/NPC was similar to Mo-DPA/NPC except for a certain reduction in size, which was consistent with the FESEM re-

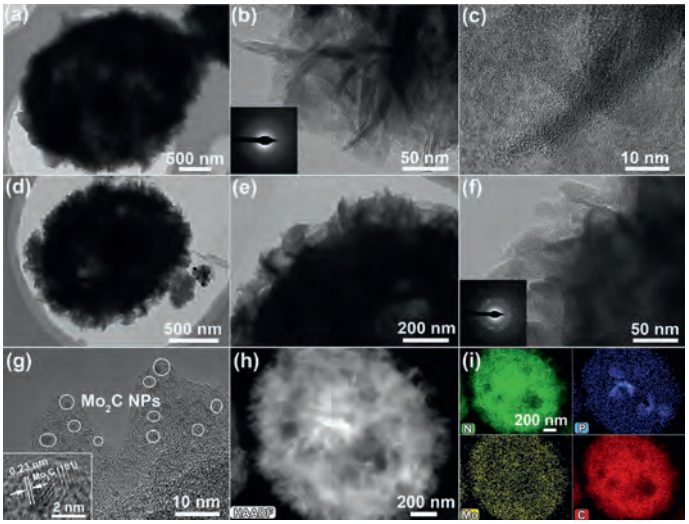

Fig. 2. (a, b) TEM and (c) HRTEM images of Mo-DPA/NPC. (d-f) TEM, (g) HRTEM, (h) HAADF-STEM and (i) EDS elementals mapping images of N,P-Mo_2C/NPC. The insets in (b) and (f) was the related SAED pattern.

sults. The polycrystalline nature of N,P-Mo_2C/NPC was confirmed by the SAED pattern (Fig. 2f). As shown in Fig. 2g, the ultrathin nanosheets were made up of numerous small nanocrystallites (less than 5 nm), which uniformly loaded in the porous carbon matrix. The reason was that the *in-situ* and restricted carburization reactions inhibit the excessive growth of crystallites, so that ultra-fine Mo_2C nanoparticles were uniformly dispersed in the carbon matrix. The typical HRTEM image of the nanoparticle (inset in Fig. 2g) clearly showed the lattice fringes spacing of 0.23 nm corresponding to the (101) lattice plane of Mo_2C. The high-angle annular dark-field scanning transmission electron microscopy (HAADF-STEM) coupled with EDS element mapping images indicated the homogeneous distribution of the N, P, Mo and C elements in N,P-Mo_2C/NPC (Figs. 2h and i).

To better understand the formation process of N,P-Mo_2C/NPC, especially the N/P diffusion process, thermal gravimetric analysis (TG) was firstly carried out with Mo-DPA/NPC precursor in Ar/H_2 atmosphere. There were three major steps of weight loss shown in Fig. 3a, and the first weight loss occurred from 40 °C to 100 °C was very small, which most likely was the loss of adsorbed water. The second weight loss was reached up to 68.2% between 278 °C to 569 °C, which was likely owing to the pyrolysis of Mo-DPA. To operando detect the gaseous species produced during calcination, a mass spectrometer was tandem with the gas outlet of thermal gravimetric analyser (TG-MS) for analyzing the gas composition. As shown in Fig. 3b, the curves demonstrated that carbonaceous and nitrogen species was released in the temperature between 278 °C and 569 °C. It was worth noting that the signal corresponding to PH_3 was not detected, which indicated that the P-doped was realized by a solid-phase diffusion process and consistent with the previous reports [36]. X-ray photoelectron spectroscopy (XPS) was used to accurate detect the surface chemical property in N,P-Mo_2C/NPC. As shown in Fig. S4 (Supporting information), P (2.16 at%), N (4.28 at%), Mo (38.81 at%) and C (54.75 at%) elements were detected in N,P-Mo_2C/NPC by the XPS survey spectrum. The high-resolution XPS spectra of P 2p was shown in Fig. 3c, the two P 2p peaks located at 132.5 and 133.3 eV were derived from the P-C and P-O bonds, respectively. The another tow peaks emerged at 128 and 129.1 eV could be assigned to the P coordinated with Mo, indicating P-Mo bonds were formed in N,P-Mo_2C/NPC [37–39]. In Fig. 3d, the peaks locating at 397.9 and 400.3 eV were ascribed to pyridinic-N and pyrrolic-N, respectively, whereas the peak located at 395.1 and 393.8 eV were associated with the N-Mo bonding state and Mo 3p, respectively [39,40]. These results confirmed N and P successfully doping into Mo_2C. The peak fitting of Mo 3d suggested the existence of two states for Mo (Fig. 3e). The Mo^{6+} species were attributed to the surface oxidation of Mo_2C in air [41], whereas the Mo^{2+} species were in accordance with the Mo in the Mo_2C. In Fig. 3f, the high resolution of C 1s for N,P-Mo_2C/NPC could be deconvoluted into four peaks centered at 283.3, 284.5, 285.5 and 288.3 eV, consponding to the bonding states of P-C, C=C, C=N and O-C=O, respectively.

The electrochemical catalytic activities of N,P-Mo_2C/NPC for HER were investigated by a three-electrode system in an alkaline solution. The effect of N/P doping content and calcination temperatures of N,P-Mo_2C/NPC on HER performance were systematically studied to obtain the optimal sample (Figs. S5 and S6 in Supporting information). To further investigate the activity of N,P-Mo_2C/NPC, the NPC, N-Mo_2C and N,P-Mo_2C as control samples were synthesized. Fig. 4a showed that the trend in the HER performance was NPC < N-Mo_2C < N,P-Mo_2C < N,P-Mo_2C/NPC < 20 wt% Pt/C. For N,P-Mo_2C/NPC, the overpotential at 10 mA/cm^2 (η_{10}) was only 84 mV, which was much smaller than those of N,P-Mo_2C (164 mV), N-Mo_2C (200 mV) and NPC (659 mV), implying that the N/P co-doping and NPC substrate were important to enhance HER activity. For confirming the reaction mechanism in the HER process,

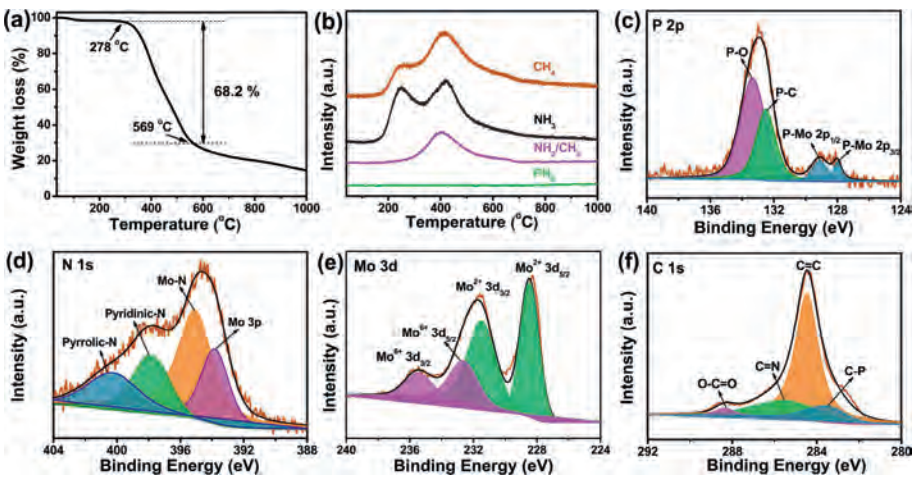

Fig. 3. (a) TG and (b) curves of gaseous decomposition products (CH_4, NH_3, NH_2/CH_3 and PH_3) derived from Mo-DPA/NPC pyrolysis process tracking by TG-MS. High-resolution XPS spectra in the (c) P 2p, (d) N 1s (overlap with Mo 3p), (e) Mo 3d and (f) C 1s regions for N,P-Mo_2C/NPC.

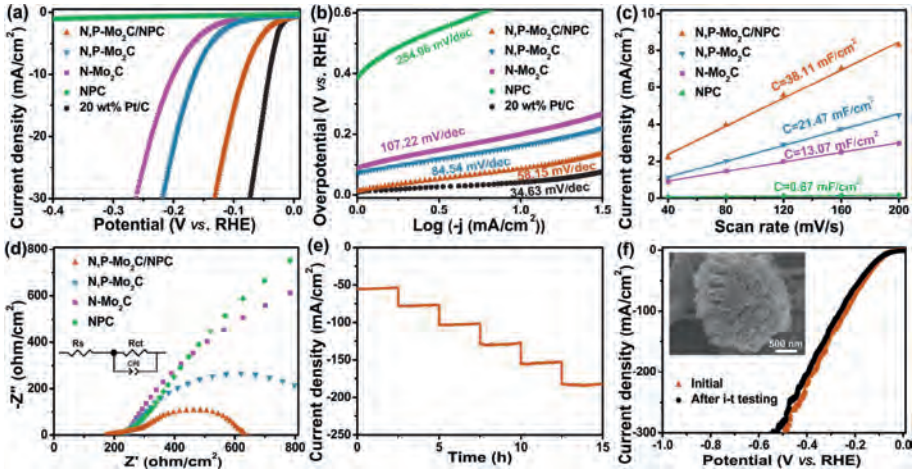

Fig. 4. (a) HER polarization curves and (b) corresponding Tafel plots of N,P-Mo_2C/NPC, N,P-Mo_2C, N-Mo_2C, NPC and 20 wt% Pt/C in 1.0 mol/L KOH (scan rate: 5 mV/s). (c) The capacitive currents as a function of scan rates. (d) Nyquist plots with 300 mV overpotential. (e) Multi-potential process of N,P-Mo_2C/NPC. The potential started from 180 mV to 430 mV, with an increment of 50 mV per 2.5 h. (f) Polarization curves of N,P-Mo_2C/NPC before and after long-time HER tests. Inset: the FESEM image of N,P-Mo_2C/NPC after *i-t* test.

the according Tafel slopes obtained by $\eta = a + b\log|j|$ were also contrasted. As shown in Fig. 4b, the Tafel slope of N,P-Mo_2C/NPC was 58.15 mV/dec, which was lower than those of N,P-Mo_2C (84.54 mV/dec), N-Mo_2C (107.22 mV/dec) and NPC (254.96 mV/dec), and slight higher than that of 20 wt% Pt/C (34.63 mV/dec), and indicating the Volmer-Heyrovsky mechanism (Eqs. 1 and 2) [42].

$$H_2O + e^- \rightarrow H_{ads} + OH^- \quad (1)$$

$$H_{ads} + H_2O + e^- \rightarrow H_2 + OH^- \quad (2)$$

The remarkable HER performance of N,P-Mo_2C/NPC ($\eta_{10} = 84$ mV, Tafel slope = 58.15 mV/dec) was surpass to, or at least comparable to, recently reported Mo_2C-based HER electrocatalysts including porous-MoC_x (128 mV, 56 mV/dec), Mo_2C nanobelts (110 mV, 49.7 mV/dec), Mo_2C/CNT (100 mV, 65 mV/dec), 30 wt%Ni-Mo_2C-R (130 mV, 49 mV/dec), Mo_2C nanotubes (112 mV, 55 mV/dec), Mo_2C@NPC (141 mV, 47.5 mV/dec) in alkaline solution and summarized in Table S1 (Supporting information). For further reveal the intrinsic HER activity of the as-obtained samples, the exchange current density (j_0) values were calculated (Fig. S7 in Supporting information). The j_0 for N,P-Mo_2C/NPC was 0.58 mA/cm^2 obviously higher than those for N,P-Mo_2C (0.17 mA/cm^2), N-Mo_2C (0.09 mA/cm^2) and NPC (0.04 mA/cm^2), indicating that the density of catalytic active sites in N,P-Mo_2C/NPC was high.

The electrochemically active surface area (ECSA) could be obtained from the electrical double-layer capacity [43,44]. In Fig. S8 (Supporting information) and Fig. 4c , the ECSA of N,P-Mo_2C/NPC was 38.11 mF/cm^2, which was lower than those of N,P-Mo_2C (21.47 mF/cm^2), N-Mo_2C (13.07 mF/cm^2) and NPC (0.67 mF/cm^2). The high ECSA of N,P-Mo_2C/NPC was beneficial to achieve large current density. Whereas, after correlation the HER activity by ECSA (Fig. S9 in Supporting information), N,P-Mo_2C/NPC still owned the lowest onset potential, which further demonstrating the high intrinsic catalytic activity of N,P-Mo_2C/NPC. The interfacial properties of electrocatalysts modified electrodes were analyzed by the measurements of electrochemical impedance spectroscopy (EIS). In Fig. 4d, the electron-transfer resistance (R_{ct}) of N,P-Mo_2C/NPC (628 Ω/cm^2) at the overpotential of 200 mV was much smaller than those of N,P-Mo_2C (945 Ω/cm^2), N-Mo_2C (3581 Ω/cm^2) and NPC (>5000 Ω/cm^2), suggesting the fastest electrocatalytic reaction rate in N,P-Mo_2C/NPC. And as the overpotential increased from 200 mV to 300 mV, the corresponding R_{ct} values of the N,P-Mo_2C/NPC decreased from 628 Ω/cm^2 to 497 Ω/cm^2 (Fig. S10 in Supporting information), indicating that the charge transfer resistance between the N,P-Mo_2C/NPC and electrolyte was accelerated at high potential.

The long-time electrocatalytic HER stability is vital to the electrocatalyst. Therefore, the current density-time curve of N,P-Mo_2C/NPC was performed over 15 h at a multi-potential process (Fig. 4e). The nearly invariant current density of constant potential of 180, 230, 280, 330, 380 and 430 mV indicated the good catalytic durability of the N,P-Mo_2C/NPC in 1.0 mol/L KOH. After testing for 15 h, the electrochemical HER performance (Fig. 4f and Fig. S11 in Supporting information) and FESEM image (inset in Fig. 4f) of N,P-Mo_2C/NPC was almost no significant change, confirming its excellent catalytic and structure stability.

The above electrocatalytic performances had indicated that N,P-Mo_2C/NPC composed of N/P doping on Mo_2C was vital to the catalytic active center. For further understanding the reason of the high catalytic activity toward HER of N,P-Mo_2C/NPC, systematic density functional theory (DFT) calculations were performed. Given the low activity of carbon toward the HER, the main active center has been demonstrated to be located at the N,P-Mo_2C. So, herein, based on prior structural data and the analysis of HRTEM, (101) surface exposing the Mo atom without/with doped of Mo_2C was constructed for our calculations and the optimized structure was shown in Figs. 5a-d. The Gibbs free energy of H* adsorption (ΔG_{H^*}) is the critical parameter to describe the HER activity. Firstly, we calculated the ΔG_{H^*} of the pure Mo_2C lattices, and found that the value of ΔG_{H^*} was relatively high (−1.01 eV), indicated the binding strength of hydrogen might be strong on the Mo_2C and poor HER activity (Fig. 5e and Fig. S12 in Supporting information). The ΔG_{H^*} value of P-Mo_2C and N-Mo_2C were −0.31 and −0.92 eV, respectively, which indicates N or P doped into Mo_2C can weaken the strong Mo-H bonding. Excitingly, the ΔG_{H^*} value of N,P-Mo_2C was close to zero (-0.03), revealing suitable H* adsorption strength. In order to further reveal the optimal ΔG_{H^*} value of N,P-Mo_2C, the Bader charge analysis was performed (inset in Fig. 5e). The N atom can get electrons from the adjacent Mo atom resulted in charge accumulation, while the P atom presented opposite process. This implies a remarkable synergistic interaction of N/P-codoped in Mo_2C. Moreover, as shown in Fig. 5f, N,P-codoping into Mo_2C could be proper enriched the electron density around the Fermi level, and made a dent in the strong Mo-H bonding. The DFT results revealed that the appropriate electron density of Mo site regulated by N,P-doping was vital to promote the HER activity.

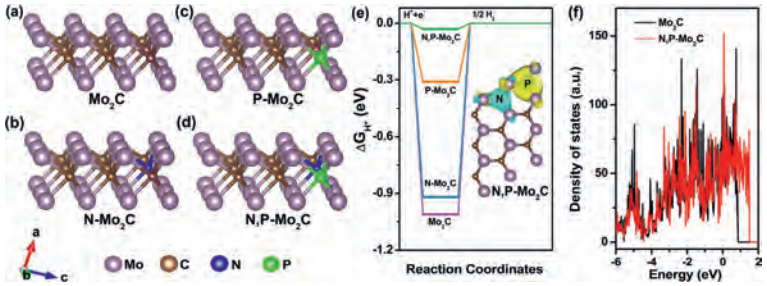

Fig. 5. The geometric configurations of (a) pristine Mo_2C, (b) N-Mo_2C, (c) P-Mo_2C and (d) N,P-Mo_2C. (e) ΔG_{H^*} calculated at the equilibrium potential of different models. Inset in (e) is the Bader charges of N,P-Mo_2C. (f) Calculated density of states for pristine Mo_2C and N,P-Mo_2C. The Fermi level is set at 0 eV.

In summary, this work adopted an idea of waste resource: upcycling the waste-yeast to prepare N,P-Mo_2C/NPC as electrocatalyst for alkaline HER. Benefit from the abundant active sites and hierarchical structure, N,P-Mo_2C/NPC displayed distinguished HER performance ($\eta = 84$ mV) in 1.0 mol/L KOH. DFT calculations further revealed that N,P-doping into Mo_2C played a key role in regulated the electron density around the Fermi level. We believe this work would not only pave the way for designing transition metal carbide composite catalysts via judicious interface engineering on the N/P configuration, but only provided a kind of idea by the resource utilization of solid waste.

Declaration of competing interest

The authors declare that they have no known competing financial interests or personal relationships that could have appeared to influence the work reported in this paper.

Acknowledgments

This work was supported by Taishan Scholars Project Special Funds (No. tsqn201812083), Natural Science Foundation of Shandong Province (Nos. ZR2019YQ20, 2019JMRH0410) and the National Natural Science Foundation of China (Nos. 51972147, 52022037, 52002145).

Supplementary materials

Supplementary material associated with this article can be found, in the online version, at doi:10.1016/j.cclet.2021.10.046.

References

[1] Z. Seh, J. Kibsgaard, C. Dickens, et al., Science 355 (2017) eaad4998.
[2] T. Takata, J. Jiang, Y. Sakata, et al., Nature 581 (2020) 411–414.
[3] Y. Wei, X. Zhang, Z. Wang, et al., Chin. Chem. Lett. 32 (2021) 119–124.
[4] H. Wu, H. Alshareef, T. Zhu, InfoMat 1 (2019) 417–425.
[5] K. Chen, S. Deng, Y. Lu, et al., Chin. Chem. Lett. 32 (2021) 765–769.
[6] G. Li, J. Yu, W. Yu, et al., Small 16 (2020) 2001980.
[7] J. Yu, A. Wang, W. Yu, et al., Appl. Catal. B: Environ. 277 (2020) 119236.
[8] T. Guo, L. Wang, S. Sun, et al., Chin. Chem. Lett. 30 (2019) 1253–1260.
[9] Y. Wei, X. Zhang, Z. Wang, et al., Chin. Chem. Lett. 32 (2021) 119–124.
[10] A. Adam, M. Suliman, H. Dafalla, et al., ACS Sustain. Chem. Eng. 6 (2018) 11414–11423.
[11] X. Chen, X. Zhen, H. Gong, et al., Chin. Chem. Lett. 30 (2019) 681–685.
[12] Z. Cao, Q. Chen, J. Zhang, et al., Nat. Commun. 8 (2017) 15131.
[13] C. Wang, F. Hu, H. Yang, et al., Nano Res. 10 (2017) 238–246.
[14] X. Li, J. Yu, J. Jia, et al., Nano Energy 62 (2019) 127–135.
[15] C. Cui, R. Cheng, C. Zhang, et al., Chin. Chem. Lett. 31 (2020) 988–991.
[16] J. Chi, Y. Chai, X. Shang, et al., J. Mate. Chem. A 6 (2018) 24783–24792.
[17] G. Zhu, L. Ma, H. Lv, et al., Nanoscale 9 (2017) 1237–1243.
[18] C. Xia, H. Liang, J. Zhu, et al., Adv. Energy Mater. 7 (2017) 1602089.
[19] W. Zhou, J. Lu, K. Zhou, et al., Nano Energy 28 (2016) 143–150.
[20] Y. Ma, C. Wu, X. Feng, et al., Energy Environ. Sci. 10 (2017) 788–798.
[21] L. Han, J. Xu, Y. Huang, et al., Chin. Chem. Lett. 32 (2021) 2263–2268.
[22] J. Yu, W. Zhou, T. Xiong, et al., Nano Res. 10 (2017) 2599–2609.
[23] Z. Wei, X. Hu, S. Ning, et al., ACS Sustain. Chem. Eng. 7 (2019) 8458–8465.
[24] L. Ma, Y. Hu, G. Zhu, et al., Chem. Mater. 28 (2016) 5733–5742.
[25] Y. Hu, X. Gao, Y. Zhu, et al., Chem. Mater. 30 (2018) 6431–6439.
[26] H. Lin, Z. Shi, S. He, et al., Chem. Sci. 7 (2016) 3399–3405.
[27] Y. Huang, Q. Gong, X. Song, et al., ACS Nano 10 (2016) 11337–11343.
[28] R. Ma, Y. Zhou, Y. Chen, et al., Angew. Chem. Int. Ed. 54 (2015) 14723–14727.
[29] Y. Chen, Y. Zhang, W. Jiang, et al., ACS Nano 10 (2016) 8851–8860.
[30] J. Tiwari, N. Dang, S. Sultan, et al., Nat. Sustain. 3 (2020) 556–563.
[31] X. Huang, X. Zou, Y. Meng, et al., ACS Appl. Mater. Interfaces 7 (2015) 1978–1986.
[32] F. Ma, B. Hao, Y. Bao, et al., Angew. Chem. Int. Ed. 54 (2015) 15395–15399.
[33] T. Xiao, A. York, H. Al-Megren, et al., J. Catal. 202 (2001) 100–109.
[34] J. Su, Y. Yang, G. Xia, et al., Nat. Commun. 8 (2017) 14969.
[35] A. Ferrari, D. Basko, Nat. Nanotech. 8 (2013) 235–246.
[36] J. Yu, G. Li, H. Liu, et al., Adv. Funct. Mater. 29 (2019) 1901154.
[37] Z. Shi, K. Nie, Z. Shao, et al., Energy Environ. Sci. 10 (2017) 1262–1271.
[38] Z. Pu, I. Amiinu, Z. Kou, et al., Angew. Chem. Int. Ed. 11 (2017) 11559–11564.
[39] L. Ji, J. Wang, X. Teng, et al., ACS Appl. Mater. Interfaces 10 (2018) 14632–14640.
[40] Y. Wang, X. Han, P. Xu, et al., Chem. Eng. J. 372 (2019) 312–320.
[41] Y. Zhu, G. Chen, X. Xu, et al., ACS Catal (2017) 3540–3547.
[42] X. Tian, P. Zhao, W. Sheng, Adv. Mater. 31 (2019) 1808066.
[43] F. Zheng, Y. Yang, Q. Chen, Nat. Commun. 5 (2014) 5261.
[44] Y. Jin, H. Wang, J. Li, et al., Adv. Mater. 28 (2016) 3785–3790.